

The photodissociation dynamics of OCIO between 306 and 370 nm: Fragment translational energy release and recoil anisotropy

Alan Furlan, Heiner A. Scheld, and J. Robert Huber

Citation: *The Journal of Chemical Physics* **106**, 6538 (1997); doi: 10.1063/1.473652

View online: <http://dx.doi.org/10.1063/1.473652>

View Table of Contents: <http://scitation.aip.org/content/aip/journal/jcp/106/16?ver=pdfcov>

Published by the [AIP Publishing](#)

Articles you may be interested in

[Overtone vibrational spectroscopy in H₂-H₂O complexes: A combined high level theoretical ab initio, dynamical and experimental study](#)

J. Chem. Phys. **137**, 084301 (2012); 10.1063/1.4732581

[Dynamics of OH radical generation in laser-induced photodissociation of tetrahydropyran at 193 nm](#)

J. Chem. Phys. **124**, 024305 (2006); 10.1063/1.2149378

[The dissociation dynamics of HeI 35 Cl \(B, v' = 2, 3\) complexes with varying amounts of internal energy](#)

J. Chem. Phys. **122**, 044318 (2005); 10.1063/1.1829971

[Molecular dynamics study of the photodissociation of OCIO in bulk liquids](#)

J. Chem. Phys. **116**, 8930 (2002); 10.1063/1.1471557

[Photodissociation dynamics of OCIO at 157 nm](#)

J. Chem. Phys. **108**, 10061 (1998); 10.1063/1.476466



The photodissociation dynamics of OCIO between 306 and 370 nm: Fragment translational energy release and recoil anisotropy

Alan Furlan, Heiner A. Scheld, and J. Robert Huber^{a)}

Physikalisch-Chemisches Institut der Universität Zürich, Winterthurerstrasse 190,
CH-8057 Zürich, Switzerland

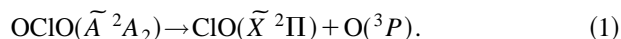
(Received 12 November 1996; accepted 22 January 1997)

The photodissociation $\text{OCIO}(\tilde{A}^2A_2) \rightarrow \text{ClO}(\tilde{X}^2\Pi) + \text{O}(^3P)$ was studied at wavelengths between 306 and 370 nm using photofragment translational energy spectroscopy. The flight time distributions and anisotropies of the recoiling fragments were measured with the photolysis wavelength tuned to 10 maxima of the structured absorption spectrum, corresponding to a vibronic excitation of the parent molecule with 9–18 quanta in the symmetric stretching coordinate on the \tilde{A}^2A_2 surface. The translational energy distributions show that the ClO fragments are created in highly inverted vibrational state distributions which become extremely broad [$\nu(\text{Cl-O}) \sim 1-15$] with increasing excitation energy. The large fraction of vibrationally hot ClO fragments produced—particularly at $\lambda < 325$ nm—could enhance various thermodynamically unfavorable atmospheric reactions in connection with ozone depletion. The main mechanistic features of the dissociation process, which account for the almost constant average translational energy and linearly increasing vibrational energy of ClO as a function of the excitation energy, can be interpreted, to a first approximation, as vibrational predissociation on the \tilde{A}^2A_2 potential energy surface involving a relatively late exit barrier. From the measured translational energies the barrier height is estimated to be about 48 kJ/mol. © 1997 American Institute of Physics. [S0021-9606(97)01716-9]

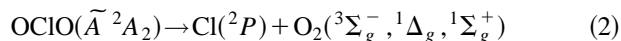
I. INTRODUCTION

Chlorine atoms and chlorine monoxide radicals (ClO) are known to play a major role in reactions responsible for atmospheric ozone depletion.¹⁻⁵ In the cold Antarctic lower stratosphere, where heterogeneous reactions on stratospheric clouds can occur, additional ozone-depleting reaction cycles are potentially important involving, among other species, ClOOC and OCIO.^{3,5,6} This possible role in the ozone depletion has stimulated extensive studies, both experimental and theoretical, on OCIO and its photodissociation in the near UV region.

Following excitation into the \tilde{A}^2A_2 state, the predominant dissociation channel of OCIO between 275 and 475 nm was found to be⁶⁻¹³



The analysis of the highly structured absorption spectrum in the near UV region has indicated that the decay is a predissociative process with the bending mode ν_2 , and at higher energy also the asymmetric stretching mode ν_3 , acting as promoting modes.¹⁴⁻¹⁶ The second decay channel



was shown to be of minor importance. This channel has a maximum yield of $3.9 \pm 0.8\%$ at $\lambda_{\text{exc}} = 404$ nm which decreases to $< 0.2\%$ at $\lambda_{\text{exc}} < 370$ nm. An interesting mode selectivity was observed for the branching ratio of these two decay channels.^{7,17} Excitation of the asymmetric stretching mode ν_3 favors ClO formation, whereas excitation of the

bending mode ν_2 enhances the efficiency of channel (2), relative to excitation of modes involving only the symmetric stretching vibration ν_1 .^{7,17}

The formation of ClOO, created by the photoisomerization $\text{OCIO} \rightarrow \text{ClOO}$ or by recombination of the primary products $\text{ClO} + \text{O} \rightarrow \text{ClOO}$ from Eq. (1), has been observed in noble gas matrices.¹⁸⁻²¹ Photoisomerization and the subsequent decay of ClOO to $\text{Cl} + \text{O}_2$ is however not important in the gas phase. The high fragment translational energy release found in the photofragment translational energy (PTS) study by Davis and Lee⁷ is an indication that the ClOO intermediate is an unlikely precursor.

The reaction dynamics of OCIO has also been studied on a femtosecond time scale using multiphoton ionization in combination with mass spectrometry.¹² On tuning the excitation laser from the vibronic band $\nu_1 = 11-17$ (352–308 nm), the bond breakage time of reaction (1) was found to change from ~ 500 to 300 fs, which is consistent with the increasing linewidths of these vibronic bands with increasing excitation energy.¹⁶ In a recent study Delmdahl *et al.*¹³ have probed the ClO photofragment from reaction (1) after excitation at 351 nm ($\nu_1 = 11$) and 308 nm ($\nu_1 = 18$) by a two-photon laser-induced fluorescence technique. At 351 nm they found the ClO fragments to be created in the vibrational states $v = 0-4$ with a moderate rotational excitation. The recoil anisotropy parameter was measured to be $\beta = 1.14$ and the population ratio of the spin-orbit states $\Pi_{3/2}/\Pi_{1/2} = 3.8 \pm 0.5$. A much higher vibrational excitation of ClO was observed at 308 nm but the rotational excitation remained similar to that at 351 nm.

From the theoretical efforts^{22,23} on the OCIO photodissociation the extensive calculations of Peterson and Werner²³

^{a)}Electronic mail: jrhuber@pci.unizh.ch

are particularly pertinent to the present work. They calculated potential energy functions of the first four doublet electronic states \tilde{X}^2B_1 , 2B_2 , 2A_1 , and \tilde{A}^2A_2 of OCIO. Their results indicate that the predissociation of the \tilde{A}^2A_2 state involves a subtle interplay between the bending and asymmetric stretching modes in the 2B_2 and 2A_1 states which couple via nonadiabatic interactions to the \tilde{A}^2A_2 state. From the predicted surface crossings of the 2A_1 with the \tilde{A}^2A_2 state, they concluded that it is the 2A_1 state which predissociates the \tilde{A}^2A_2 state through spin-orbit coupling. Following this initial crossing to the 2A_1 potential surface, the molecule is predicted to dissociate to ClO and O (1) through the linear configuration or cross to the 2B_2 surface by vibronic Herzberg-Teller interactions, where dissociation to ClO+O proceeds by the asymmetric stretching vibration.

The present study deals with the excitation wavelength dependence of the kinetic energy E_T of the primary fragments emerging from reaction (1) and their recoil anisotropy β . In the wavelength range between ~ 370 and 306 nm the excitation was tuned to the absorption bands of the symmetric stretching mode progression from (9,0,0) to (18,0,0) and $E_T(\lambda)$ and $\beta(\lambda)$ of the photofragments were measured by using photofragment translational energy spectroscopy.²⁴⁻²⁷

II. EXPERIMENT

The experiments were carried out with a photofragment translational energy spectrometer which has been described in detail elsewhere.^{28,29} It consists of a rotatable, pulsed molecular beam source, a 34.5-cm-long drift tube, and a quadrupole mass spectrometer for mass filtering and detection. The photolysis laser beam crossed the molecular beam at a distance of 65 mm from the piezoelectric pulsed nozzle. Laser pulses of 0.5–5 mJ ($\Delta\tilde{\nu}=0.15\text{ cm}^{-1}$, $\tau\sim 6\text{ ns}$) were obtained by frequency doubling the output of a Nd:YAG-pumped dye laser (Scanmate 2E). The laser beam was slightly focused to a $2\times 2\text{ mm}^2$ spot at the intersection with the molecular beam.

OCIO was generated by passing Cl_2 over NaClO_2 . The NaClO_2 contained 2 mbar of H_2O to catalyze the reaction.³⁰ After completion of the reaction, the yellow product was passed through an additional U-tube filled with NaClO_2 and glass beads, and cooled with ice water to remove H_2O . Accurate determinations of flight times and fragment anisotropies required a high stability of the molecular beam conditions throughout the measurement period. For each measurement 36 mbar of fresh OCIO were produced and transferred to a container, which was then filled with He to a total pressure of 800 mbar and automatically held at constant pressure. The velocity distribution of the molecular beam pulse $f(v)\sim v^2 \exp[-(v-v_s)^2/\alpha^2]$ was determined before and after each measurement, using a chopper wheel synchronized with the pulsed valve. The chopper data for $f(v)$ were checked by laser-induced hole burning.³¹ The stream velocity v_s and the width α of the OCIO/He mixture were measured to be 1240 ± 35 and 70 ± 4 m/s, respectively. Because OCIO is subject to decomposition upon contact with metal, the experiments were performed with a metal-free inlet sys-

tem and a specially designed TeflonTM molecular beam valve, which has been described elsewhere.³² This enabled us to maintain a constant OCIO concentration of $4.5\%\pm 0.2\%$ in He for 2–3 h. It should be noted that OCIO is explosive at concentrations in excess of 10% atmospheric pressure.³⁰

The recoil anisotropies $\beta(\lambda_{\text{exc}})$ were measured by means of a half-wave plate (B. Halle, Berlin). The degree of the laser polarization was found to be $>97\%$ over the wavelength range used. Each anisotropy measurement was carried out at six different polarization angles with 5000 laser shots each. This procedure was repeated four times to minimize the influence of long-term drifts and the runs were normalized to the average laser power. The intensity $I(\epsilon)$ measured at the different polarization angles ϵ , where ϵ is the angle between the electric field vector E and the detector axis, were fitted to the expression^{33,34}

$$I(\epsilon) = A\{2 + \beta[3 \cos^2(\epsilon - \epsilon_0) - 1]\} \quad (3)$$

and thus provided the anisotropy parameter β . Here A is a normalization constant and ϵ_0 is an offset angle, which accounts for the difference in the direction of the fragments in the lab-fixed system and the center-of-mass (c.m.) system. The offset angle was measured at each chosen wavelength separately, since it may change with the kinetic energy of the fragments.^{33,34} Unpolarized time-of-flight (TOF) data were obtained by adding two polarized spectra recorded at perpendicular polarization angles, or alternatively by using a Cornu pseudodepolarizer.

To avoid saturation and multiphoton effects, the laser pulse energy was kept at ≤ 1.0 mJ for all measurements. This corresponds to a saturation parameter (absorption cross section \times fluence) $\sigma F = 0.52$ for the (11,0,0) level ($\sigma = 1.2 \times 10^{-17}\text{ cm}^2$)³⁵ and $\sigma F = 0.14$ for the (18,0,0) level ($\sigma = 3.6 \times 10^{-18}\text{ cm}^2$).³⁵ Within the pulse energy range 0.5–3.0 mJ the signal intensity depended linearly on the laser power, indicating that the observed photodissociation was a single-photon process; multiphoton contributions were negligible under our experimental conditions.

A time offset of $3.9\ \mu\text{s}(e/m)^{1/2}$ has been subtracted in all of the TOF spectra shown in order to correct for the transit time of the ions through the mass filter.^{28,29}

III. RESULTS

A. Measurements with unpolarized light

Figures 1(a) and 2(a) show the TOF distributions recorded with the mass spectrometer set to the fragment mass $m/e = 51$ using different scattering angles Θ . The signal at this mass setting can be unambiguously assigned to the ^{35}ClO fragment formed in process (1). The solid line represents the best fit calculated by a forward convolution procedure,³⁶ and the corresponding translational energy distributions $P(E_T)$ of the fragment pairs of channel (1) are displayed in Figs. 1(b) and 2(b). Comparison of Fig. 1 with Fig. 2 reveals the high sensitivity of the translational energy

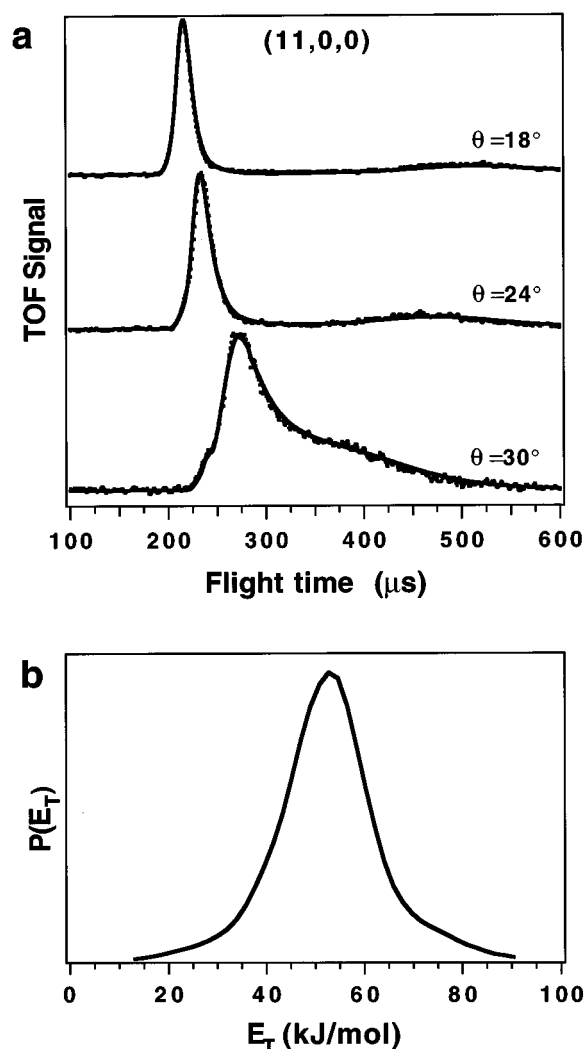


FIG. 1. (a) Unpolarized TOF distributions of ClO fragments measured at $m/e=51$ with $\Theta=18^\circ$, 24° , and 30° from OCIO excited to the (11,0,0) vibronic level in the \tilde{A}^2A_2 state. (b) Translational energy distribution $P(E_T)$ obtained from a forward convolution fitted to the three TOF spectra shown above.

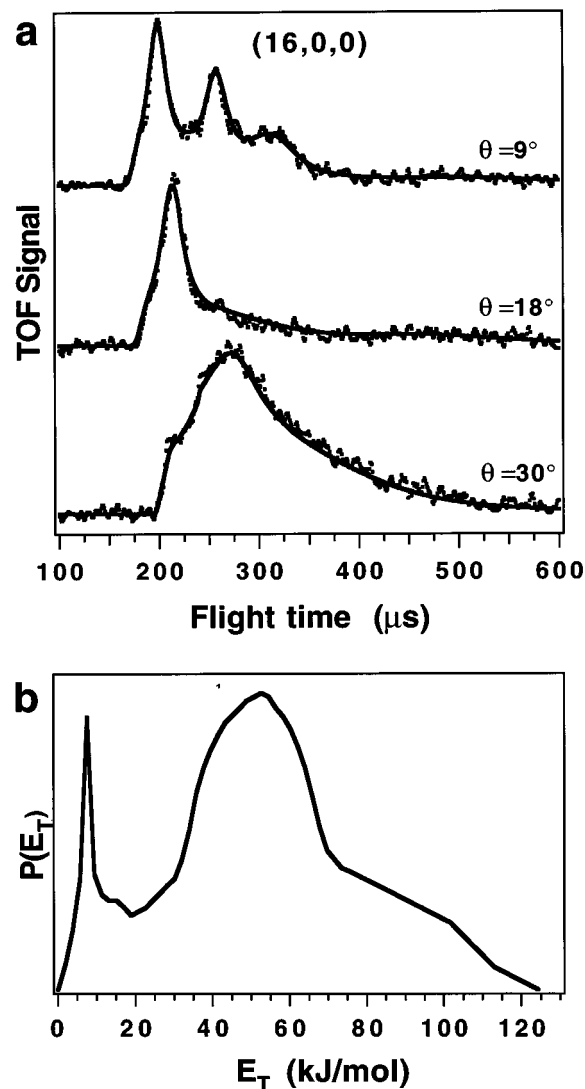


FIG. 2. (a) Unpolarized TOF distributions of ClO fragments measured at $m/e=51$ with $\Theta=9^\circ$, 18° , and 30° from OCIO excited to the (16,0,0) level. (b) Translational energy distribution $P(E_T)$ obtained from the three TOF spectra shown above.

distribution with respect to the excitation energy or the excited overtone ν_1^i in the \tilde{A}^2A_2 state, here as examples (11,0,0) and (16,0,0).

The threshold scattering angle Θ_{thr} is determined by the fastest and hence vibrationally and rotationally cold ClO fragments. According to the Newton diagram, Θ_{thr} is 46° at 360 nm and 70° at 308 nm but in our experiment the TOF signal was found to be very weak at $\Theta > 35^\circ$. The fraction of vibrationally cold ClO products is obviously very low (see below). Close to the molecular beam at $\Theta > 20^\circ$ the TOF spectra exhibited contributions from parent molecules. This background could however be subtracted on a shot to shot basis by leaving every second molecular beam pulse unphotolyzed.

We performed TOF measurements at ten different excitation wavelengths from 368.63 to 306.93 nm which correspond to excitation into the symmetric stretching mode (9,0,0) to (18,0,0) in the \tilde{A}^2A_2 state of OCIO. At each wave-

length three or four TOF spectra at different Θ (9° , 18° , 24° , and/or 30°) were recorded. These extended sets of TOF spectra allowed an accurate determination of $P(E_T)$. Figure 3 shows the TOF spectra after excitation into the vibronic bands (14,0,0) to (18,0,0), illustrating the change from a single peak spectrum centered at about $200 \mu\text{s}$ flight time to a considerably broadened spectrum with the fastest peak remaining at $\sim 200 \mu\text{s}$. These TOF spectra correspond to the center-of-mass (c.m.) translational energy distributions $P(E_T)$ given in Fig. 4. The roughly Gaussian shaped distribution obtained with (9,0,0) excitation broadens with increasing excitation energy, an effect which becomes clearly apparent between the (13,0,0) and (15,0,0) excitation. In this context it is noted that Davis and Lee¹⁷ measured corresponding TOF spectra at lower excitation energies except those with excitation into the (9,0,0) and (10,0,0) band. The $P(E_T)$ distributions from these latter measurements agree

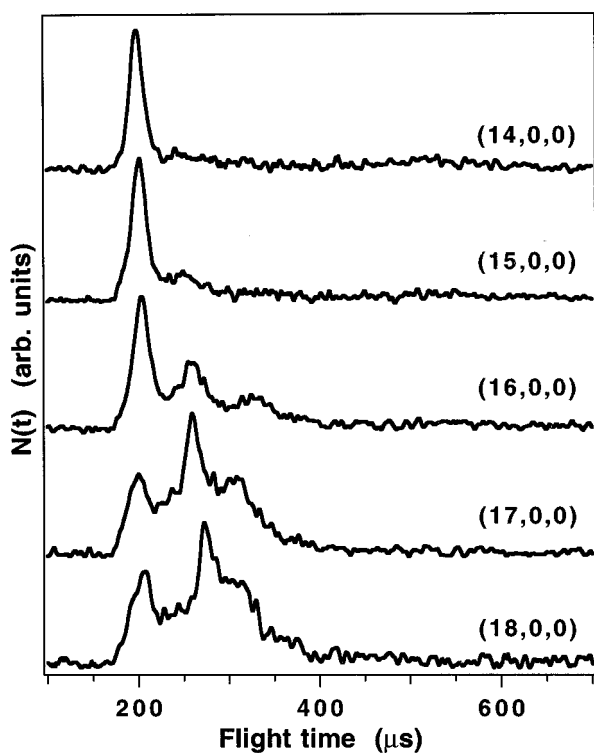


FIG. 3. Translational energy distributions $P(E_T)$ obtained from excitation to the vibronic levels (9,0,0)–(13,0,0) in the \bar{A}^2A_2 state of OCIO. Each of the curves was fitted to TOF spectra measured at $\Theta=18^\circ$, 24° , and 30° .

very well with our findings of Fig. 4 (bottom).

The intensity of the TOF spectra in Figs. 1–3 reflects the population of the rovibrational states of the OCl fragment but also depends on the electron impact ionization cross section σ_{ion} and the fragmentation pattern. We have assumed that these parameters remain constant for the different vibrational excitation of the ClO fragment. For modest vibrational excitation this has been confirmed in the work of Davis and Lee.¹⁷ TOF spectra of the counterfragments O, which carry the same information as those of ClO due to momentum conservation, would obviously not require such an assumption. The poor signal-to-noise ratio of the TOF spectra at $m/e=16$ prevented us from definitively confirming the independence of these parameters also for higher excited vibrational states of ClO. We are, however, confident that this is the case since σ_{ion} is relatively insensitive to fragment vibrational excitation at high electron impact energies (160 eV) and the dissociation pattern is not expected to change for the strongly bound ClO^+ ion which has a dissociation energy of about 470 kJ/mol.³⁷

From the $P(E_T)$ distribution of Fig. 4 the dissociation energy D_0 of reaction (1) and the internal energy distribution of the OCl fragment can be extracted. Energy conservation requires the available energy to be

$$E_{\text{avl}} = h\nu + E_{\text{int}}(\text{OCIO}) - D_0, \quad (4)$$

where $h\nu$ is the photon energy and $E_{\text{int}}(\text{OCIO})$ the internal energy of the parent molecule. The latter can be neglected under our supersonic expansion conditions. The fragments

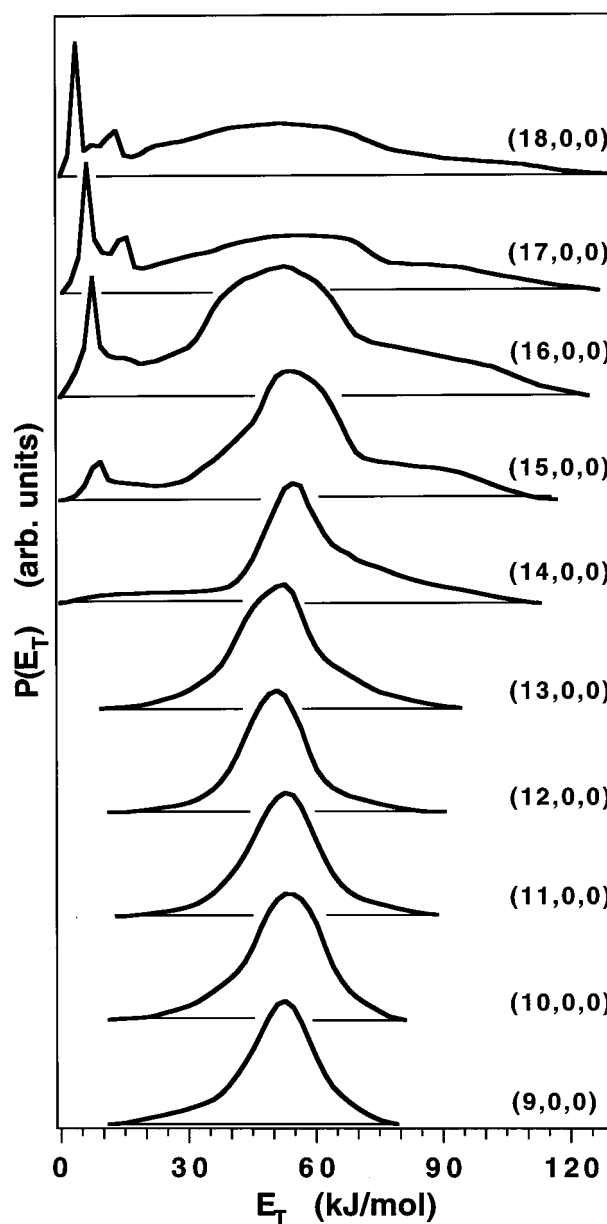


FIG. 4. Translational energy distributions $P(E_T)$ for the levels (14,0,0)–(18,0,0). Each of the curves was fitted to TOF spectra measured at $\Theta=9^\circ$, 18° , and 30° .

with the highest translational energy E_T^{max} are those which possess no internal energy, i.e., they are formed in the vibrational, rotational, and spin–orbit ground state. Based on the previous results we therefore expect, at least for the lowest applied excitation energies, the fastest fragments of the $P(E_T)$ distribution to obey the relationship $E_{\text{avl}} \equiv E_T^{\text{max}} = h\nu - D_0$, which provides the dissociation energy. From the distributions (9,0,0) to (12,0,0) in Fig. 4 we thus find $D_0 = 248 \pm 2$ kJ/mol. This is in excellent agreement with the value of 246.9 ± 0.8 kJ/mol recently reported by Davis and Lee.¹⁷

For the product pair ClO ($^2\Pi_{3/2}$) and O (3P_2) in their electronic ground states E_{int} is comprised of the vibrational

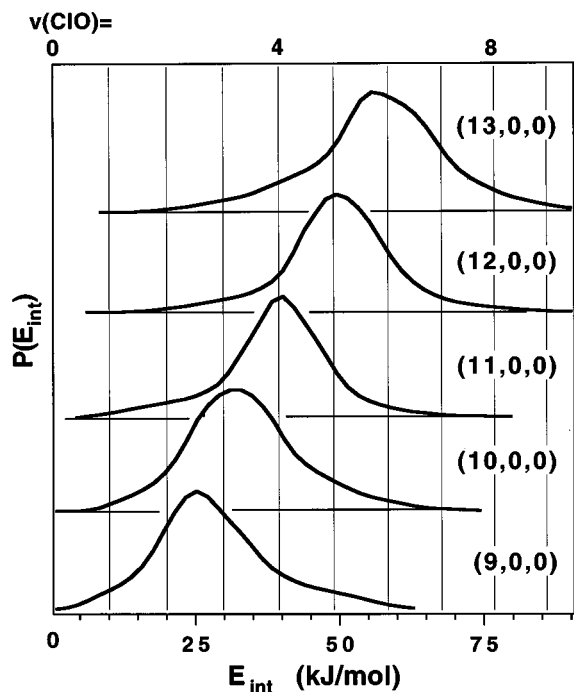


FIG. 5. Internal energy distributions $P(E_{\text{int}})$ for the vibronic levels (9,0,0)–(13,0,0), obtained by using a dissociation energy $D_0(\text{O}-\text{ClO})=247$ kJ/mol. Since the contribution of rotational excitation to $E_{\text{int}}=E_{\text{avl}}-E_T$ was found to be small [$\langle E_{\text{rot}} \rangle=7.5$ kJ/mol (Ref. 13)] E_{int} is roughly equivalent to the vibrational excitation of the ClO fragment. The vibrational energy spacing is indicated by the grid (see the text).

and rotational energy of the ClO fragment. A contribution from electronic excitation may arise from ClO where the two spin-orbit states $\Pi_{3/2}$ and $\Pi_{1/2}$ are separated by 318 cm^{-1} .³⁸ For the O atom the spin-orbit states lie 227 cm^{-1} (3P_0) and 158 cm^{-1} (3P_1) above the 3P_2 ground state. Although we are able to resolve only the vibrational structure, providing the rotational distribution is not too broad, some of the finer details are revealed at low translational energy (Fig. 4), or correspondingly at high internal energy (Figs. 5 and 6), where the resolution is greatest and the rotational excitation is low. This is nicely demonstrated in Fig. 6 for the four highest excited vibrational states ($v=12-15$) of ClO the structure of which appears as clearly distinguishable peaks separated by ~ 650 cm^{-1} .

B. Polarized measurements and recoil anisotropy

Figure 7 displays the TOF signal intensity I measured as a function of the laser polarization angle ϵ ³⁹⁻⁴¹ and expressed by Eq. (3).³³ To illustrate this dependence we selected the data for excitation into the (10,0,0) and (16,0,0) vibronic absorption bands of OCIO (\tilde{A}^2A_2), which gives rise to a strong fragment anisotropy change. Only the result for one run is shown but every run was repeated three times. The dependence of the anisotropy parameter β on the flight time was found to be small, $|\Delta\beta(t)| \leq 0.15$, but the variation of the fitted offset angle ϵ_0 with flight time was substantial. Especially for flight times >300 μs an accurate determination of ϵ_0 was difficult. Under these conditions the c.m. frag-

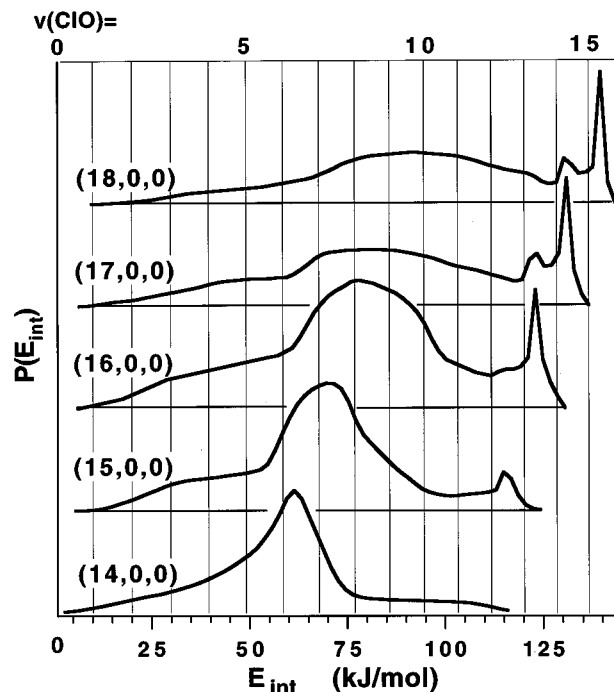


FIG. 6. Internal energy distributions $P(E_{\text{int}})$ for the vibronic levels (14,0,0)–(18,0,0). See the caption of Fig. 5 and the text.

ment velocity \mathbf{u} (which defines ϵ_0) is not much greater than the threshold velocity required for detection, and as a consequence ϵ_0 is subject to large scatter. For these reasons we restricted our anisotropy measurements to the fastest ClO fragments at any given excitation wavelength, more specifically, only the fragments arriving within an interval of 20 μs after the onset of the TOF signal were analyzed. The scattering angle Θ was kept constant at 18° . The β values derived from these measurements are given in Fig. 8, revealing the dependence on the excitation wavelength. Between ~ 370

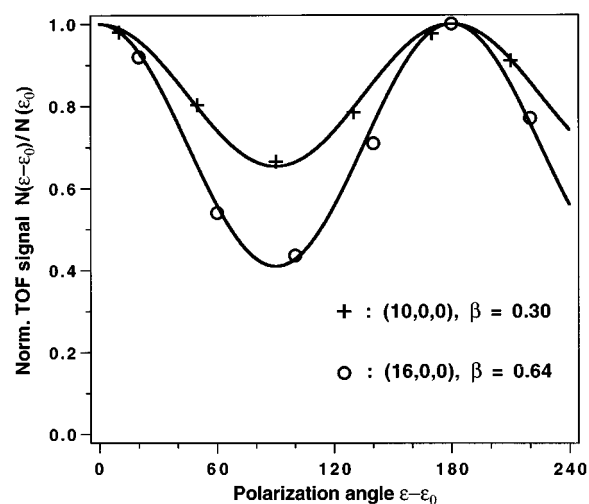


FIG. 7. Dependence of the ClO fragment signal on the polarization angle ϵ for the OCIO vibronic levels (10,0,0) and (16,0,0). The solid lines are fits with $\beta=0.30$ and $\beta=0.64$, respectively.

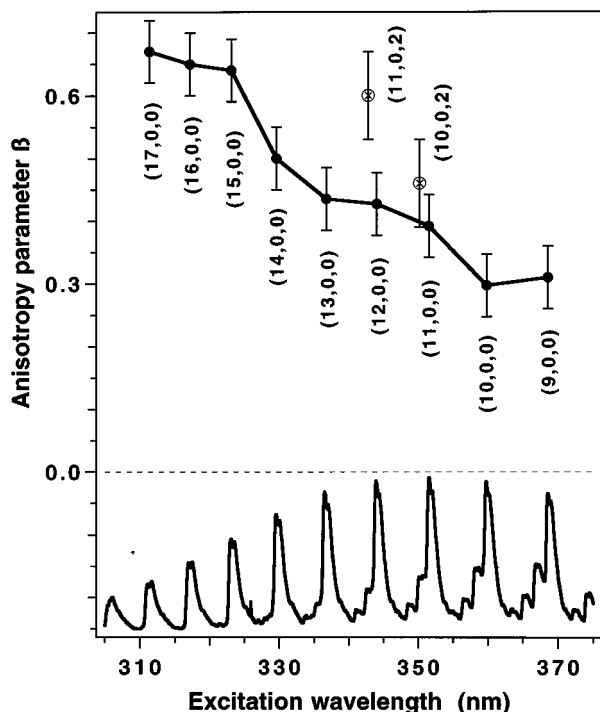


FIG. 8. Anisotropy parameter β measured at $m/e=51$ with the photolysis wavelength tuned to the OCIO vibronic levels (9,0,0)–(17,0,0). The lower panel shows a part of the OCIO absorption spectrum dominated by the symmetric stretching mode ν_1 .

nm, with excitation into the symmetric stretching mode (9,0,0), and ~ 310 nm (17,0,0), β increases from 0.3 to 0.6. Two exploratory measurements including the asymmetric stretching mode (10,0,2) and (11,0,2) exhibit a tendency to slightly higher β values.

A rough estimation of the dissociation lifetime can be obtained from the anisotropy parameters.^{41–43} For dissociation occurring instantaneously after photon absorption, $\beta = 2P_2(\cos \chi)$, where P_2 is the second-order Legendre polynomial and χ the angle between the electronic transition moment $\boldsymbol{\mu}$ and the recoil direction. In the case of OCIO the $\tilde{A}^2A_2 \leftarrow \tilde{X}^2B_1$ transition⁹ is induced by $\boldsymbol{\mu}$ lying in the molecular plane and parallel to the line connecting the two O atoms (C_{2v} molecular symmetry). The equilibrium bond angle in the \tilde{A}^2A_2 state is 107° ,²³ so that the ejection of the O atom along the breaking Cl–O bond yields $\chi = (180 - 107)/2$. Under these conditions the maximum value of β , which corresponds to a bond rupture proceeding much faster than a molecular rotation, is $\beta_{\max} = 0.93$. Providing $\boldsymbol{\mu}$ is well defined as assumed above, a reduction of β_{\max} can be ascribed to rotation of the parent molecule prior to dissociation. Following the treatment of Wilson and Busch⁴¹ we calculated the dissociation lifetime τ from the β values given in Fig. 8 by assuming a rotational temperature of the molecule in the beam of $T_{\text{rot}} = 40$ K [Eq. (5) in Ref. 42]. Because the uncertainty in T_{rot} introduces a relatively large error in τ , we performed the calculation also for $T_{\text{rot}} = 20$ and 80 K. The result is shown in Fig. 9. For two widely different β values, measured for excitation into the (9,0,0) and (17,0,0) band of

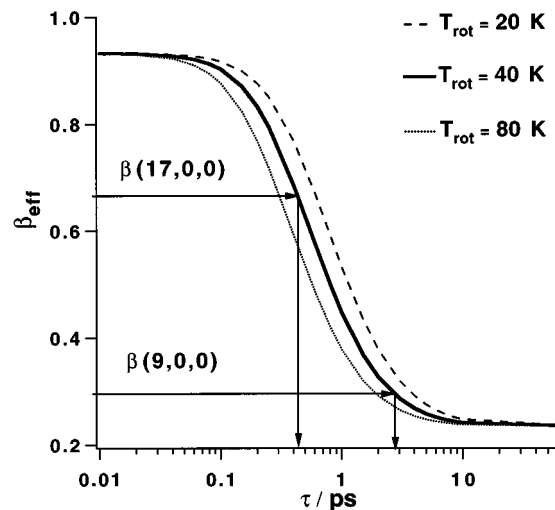


FIG. 9. The measured anisotropy β as a function of the lifetime of the excited OCIO molecule. The curves were calculated assuming for the parent molecule $T_{\text{rot}} = 20, 40,$ and 80 K, and a moment of inertia $I_{\text{eff}} = 9.2 \times 10^{-46}$ kg m², which corresponds to the average of I_a and I_b in the ground electronic state of OCIO. The vertical lines indicate the lifetimes calculated for $\beta(10,0,0) = 0.30$ and $\beta(17,0,0) = 0.67$ and $T_{\text{rot}} = 40$ K.

the \tilde{A}^2A_2 state, τ is found to be 2.5 and 0.45 ps, respectively, for $T_{\text{rot}} = 40$ K. Since any state mixing in the absorption or during the dissociation process may lead to a depolarization and hence to a smaller β value than without, these lifetime estimates must be considered upper limits.

IV. DISCUSSION

A. Energy distribution and alignment

The present investigation deals with the predissociation process (1), where the applied excitation energies allow access to the oxygen 3P_J state only. We first discuss the findings on the translational energy distribution of the fragment pair ClO+O in comparison with the results previously reported.^{12,13,17} Figure 4 presents a survey of the c.m. translational energy distributions obtained at ten different excitation energies covering a range of 66.3 kJ/mol (5545 cm^{-1}). While the distribution broadens with increasing excitation energy, the average translational energy $\langle E_T \rangle$ appears to remain roughly constant at a value of 50–55 kJ/mol [see also Figs. 1(b) and 2(b) as well as Table I]. The analysis confirms this expectation as demonstrated with the plot $\langle E_T \rangle$ vs $E_{\text{exc}} = h\nu$ in Fig. 10. Since $E_{\text{avl}} = \langle E_T \rangle + \langle E_{\text{int}} \rangle$, the almost constant translational energy release implies that the average internal energy $\langle E_{\text{int}} \rangle$ increases approximately linearly with $E_{\text{avl}} = h\nu - D_0$. The increase in excitation energy is therefore deposited into internal energy of the fragments. From their measurements of the state populations of the ClO fragment after excitation at 351 nm, Delmdahl *et al.*¹³ found a population ratio for the spin–orbit states of $P(^2\Pi_{3/2}) : P(^2\Pi_{1/2}) \sim 4$, which corresponds to an excitation energy of $< 70 \text{ cm}^{-1}$, and a Boltzmann distribution of 480 K for the rotational states. No corresponding experimental data for the spin–orbit states $^3P_{0,1,2}$ of the O fragment are available but

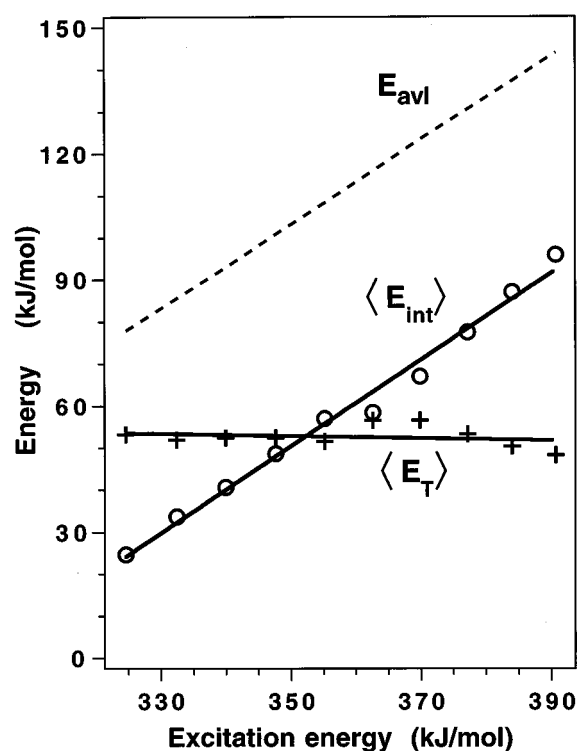


FIG. 10. Average internal energy $\langle E_{int} \rangle$ and translational energy $\langle E_T \rangle$ of the fragments as a function of the excitation (photolysis) energy $h\nu$. E_{avl} is obtained with $D_0 = 247$ kJ/mol.

their contribution to E_{int} will be very small since even for a statistical distribution the excitation energy is <80 cm^{-1} . The internal energy $\langle E_{int} \rangle$ vs E_{exc} displayed in Fig. 10 represents therefore $\langle E_{int} \rangle = \langle E_{vib} \rangle + \langle E_{rot} \rangle$ of the ClO fragment where a small contribution of <200 cm^{-1} for spin-orbit excitation has been neglected. The rotational energy at 351 nm, measured for ClO($v=0$), was reported to be ~ 7.8 kJ/mol (~ 650 cm^{-1}) and appeared to be similar at 308 nm.¹³ Compared to $\langle E_{int} \rangle$ given in Fig. 10 and Table I, this contribution from the rotational excitation is small and is not ex-

TABLE II. Available energy and detailed fragment energy partitioning.

ν_1	E_{avl} kJ/mol	$\langle E_T \rangle$ kJ/mol (%)	$\langle E_{vib} \rangle$ kJ/mol (%)	$\langle E_{rot} \rangle$ kJ/mol (%)
11	92.9	52 (56)	~ 33 (35)	~ 8 (9) ^a
18	144	48 (33)	~ 88 (61)	~ 8 (6) ^a

^aReference 13.

pected to increase in higher vibrational levels of ClO. Based on these findings, we conclude that the internal energy is mainly vibrational excitation E_{vib} and that the increase in photon energy is mainly channeled into the vibrational degree of freedom of the ClO fragment. Thus after excitation of (11,0,0) and (17,0,0) the partitioning of E_{avl} into E_{vib} increases from 35% to 61% while E_T decreases from 56% to 33% assuming E_{rot} to be constant at ~ 7.8 kJ/mol. Table II gives the detailed energy partitioning at these two excitation energies. The present measurements yield a considerably higher value for $\langle E_T \rangle$ at 351 nm (11,0,0) than the Doppler profile LIF results¹³ (52 vs 23 kJ/mol). This is partly due to the different choices of $D_0(\text{O}-\text{ClO})$.

The vibrational excitation of the ClO fragment with respect to the reaction channel leading to ClO (${}^2\Pi_{3/2}$) and O (3P_2) in their spin-orbit ground states is exhibited in Figs. 5 and 6. The Cl-O vibrational quanta up to $v=16$ are indicated on top of the figures and a grid complements this information. The vibrational energy spacings include the anharmonicity.³⁸ The rotational excitation of each vibrational state, superposition with weaker $P(E_{int})$ distributions contributed by ClO and O in excited spin-orbit states, and the resolution of our apparatus²⁹ prevent the vibrational structure from becoming apparent except for excitation above (14,0,0). There the vibrational bands of the ClO stretch $v=12, 13, 14$ and 15 are clearly discernible and manifest a spacing of ~ 650 cm^{-1} , which agrees with the expected vibrational frequencies of such high excitation.³⁸ The appearance of this structure, which is due to a decreased rotational excitation of the ClO fragment, being now $E_{rot} < 200$ cm^{-1} as

TABLE I. Available energy, energy partitioning, and anisotropy.

$(\nu_1, 0, 0)$	λ_{exc} (nm)	E_{exc} ^a	E_{avl} ^{ab}	$\langle E_T \rangle$ ^a	$\langle E_{int} \rangle$ ^a	$E_{int} \geq E^{a,c}$		β
						20%	10%	
9	368.84	324.3	77.4	52 (68)	25	36	43	0.31
10	360.1	332.1	85.2	52 (61)	34	42	47	0.30
11	352.04	339.7	92.4	52 (56)	40	46	52	0.39
12	344.13	347.5	100.6	52 (52)	49	57	63	0.43
13	337.01	354.9	108.0	54 (50)	57	67	74	0.44
14	329.99	362.4	115.5	56 (49)	58	70	82	0.50
15	323.37	369.9	123.0	56 (46)	67	82	99	0.64
16	317.23	377.0	130.1	53 (41)	77	104	116	0.65
17	311.67	383.7	136.8	50 (37)	87	120	128	0.67
18	306.21	390.6	144.0	48 (33)	96	128	137	

^aAll energies in kJ/mol; values in parenthesis are in percent of E_{avl} .

^bAvailable energy assuming a dissociation energy $D_0(\text{OClO}) = 247$ kJ/mol.

^c20% and 10% of the ClO fragments, respectively, have internal energies exceeding the values given in the table.

inferred from the bandwidth, also indicates that the contribution from spin-orbit excited fragments must be small.

The lifetimes derived from the β values which were measured for excitation to states of the ν_1 progression from (9,0,0) to (17,0,0) are 2.5–0.45 ps and they represent upper limits. These values were obtained with the assumption that the initial polarization alignment is given by the $\tilde{A}^2A_2 \leftarrow \tilde{X}^2B_1$ transition without admixture from the 2B_2 and 2A_1 neighboring excited states as inferred from an analysis of the jet-cooled high-resolution absorption spectrum.⁴⁴ Because these lifetimes τ are calculated with a simple impulsive model in which the crucial bending angle in OCIO(2A_2) is fixed during the bond-breaking process, they are only rough estimates. Nevertheless the increase in β with increasing E_{exc} (Fig. 8) is most likely due to a decreasing τ . Femtosecond real-time probing¹² as well as high-resolution linewidth measurements¹⁶ indicate the same effect. Baumert *et al.*¹² reported a biexponential decay of the OCIO⁺ signal. The faster decay component was attributed to vibrational predissociation on the \tilde{A}^2A_2 potential energy surface (PES) and the slower one to a decay on either the 2B_2 or 2A_1 PES, or the ground state surface \tilde{X}^2B_1 . Excitation of the (11,0,0) vibronic level yielded a decay time being about a factor of 2 greater than excitation of the (17,0,0) level, i.e., $\tau \approx 500$ and 300 fs, respectively. However, the parent-ion signal recorded in these measurements does not distinguish between the parent molecule decaying due to photodissociation and becoming spectroscopically dark owing to, e.g., internal conversion. The decay signal could therefore represent the sum of various decay processes (including the decay to Cl+O₂) so that the measured lifetime would be a lower limit for the OCIO dissociation (1). Linewidth measurements of Richard *et al.*^{16,44} provided lifetimes in the wavelength region >400 nm where single rotational lines are at least partly resolved. The highest vibronic band with some resolved rotational structure, the (9,0,0) band, showed widths of $\approx 1.2 \text{ cm}^{-1}$ (full width at half-maximum), which correspond to $\tau \approx 4$ ps. Compared with the results of these femtosecond and high-resolution studies the lifetimes derived from the β values are, considering the uncertainties involved, in reasonable agreement.

B. Mechanistic aspects

In the present experiments, photoexcitation from the ground state prepares OCIO in the symmetric stretching mode on the \tilde{A}^2A_2 potential energy surface. According to the most recent results of *ab initio* calculations by Peterson and Werner,²³ this PES is bound along the coordinates of the symmetric stretching and the bending mode. Along the asymmetric stretching coordinate a small barrier of about 3000 cm^{-1} separates the Franck-Condon (FC) or excitation region from the repulsive surface of the exit channel. All the excitation energies applied in the present work exceed the threshold of $\sim 25\,000 \text{ cm}^{-1}$ (3.1 eV) required to overcome this barrier on the \tilde{A}^2A_2 PES and hence give access to a direct decay to ClO+O according to reaction (1). This excitation condition may allow a discussion of the predissocia-

tion mechanism to be confined to the 2A_2 PES. The influence of the predicted spin-orbit coupling between the 2A_2 and 2A_1 states and the vibronic coupling of the latter to the 2B_2 state is thereby neglected. At lower excitation energy (<3.1 eV), where the atmospherically important reaction (2) leading to Cl+O₂ reaches its maximum yield ($\sim 4\%$ ¹⁷), the direct decay channel to ClO+O on \tilde{A}^2A_2 is predicted to be closed so that coupling to the lower lying 2A_1 and 2B_2 PES becomes necessary for dissociation to occur. Under our conditions, however, coupling to the 2B_2 state appears minor because no Cl+O₂ products were detected ($<0.2\%$ ¹⁷), which is predicted to be a characteristic feature of the 2B_2 decay. Furthermore the absence of a barrier on the 2B_2 PES²³ along the “reaction coordinate” (the asymmetric stretch) is hard to reconcile with our translational energy distributions (see below) as well as the moderate rotational excitation of the ClO fragment.¹³ The latter is expected to be high, as along the bending coordinate of OCIO the 2B_2 PES shows the minimum energy at a small angle of $\sim 90^\circ$ which gives rise to a high torque. The neglect of an interaction with the 2A_1 surface is probably more severe. The topography of this surface along the asymmetric coordinate is similar to that of the \tilde{A}^2A_2 PES but differs along the bending angle.²³ This coordinate is calculated to show only a small barrier ($\sim 0.3 \text{ eV}$ ²³) to dissociation so that the bending motion may act as a promotor for dissociation at sufficient excitation energies. Coupling between the \tilde{A}^2A_2 and 2A_1 surfaces is however anticipated to introduce a depolarization of the recoil anisotropy. Since the reduction of our measured β values (Fig. 8) from $\beta_{\text{max}} \sim 0.9$ was found to be consistent with the dissociation lifetime, evidence for a strong 2A_2 – 2A_1 coupling has not been found. Therefore, a discussion of our photodissociation results confined to the initial 2A_2 surface is attempted.

A schematic 2A_2 PES based on the *ab initio* results²³ is depicted in Fig. 11. The wave packet, initially prepared in the FC region of the excited PES, moves along the symmetric stretching coordinate \mathbf{r} and is reflected from the potential back to the FC region.⁴⁵ Within the potential well, defined by the two symmetrically positioned barriers along $r(\text{Cl-O})$, the wave packet is then expected to move in elliptical cycles mainly along \mathbf{r} leaking over the barrier into the exit channels. The residence time of the wave packet within the inner region of the PES around the FC point would thus determine the dissociation time, which was measured to be in the range of 300–500 fs depending on the ν_1 overtone. The wave packet escapes preferentially with a large amplitude motion into the exit channel giving rise to high vibrational excitation of the ClO fragment. Moreover, the experiments show the vibrational state distribution to be strongly inverted and extremely broad at high excitation energy (Fig. 6). The equilibrium bond distance $d(\text{Cl-O})$ in OCIO (2A_2) is 1.627 \AA ,²³ the corresponding one in the ClO (\tilde{X}) fragment is 1.57 \AA .³⁸ This fact leads to a minimum energy reaction path from the FC point to the separated fragments which is almost parallel to the $r(\text{Cl-O})$ reaction coordinate. This implies that there should be only a small vibrational-translational interaction⁴⁵ with respect to the ClO vibration of the emerging fragment and the translational motion along the reaction coordinate.

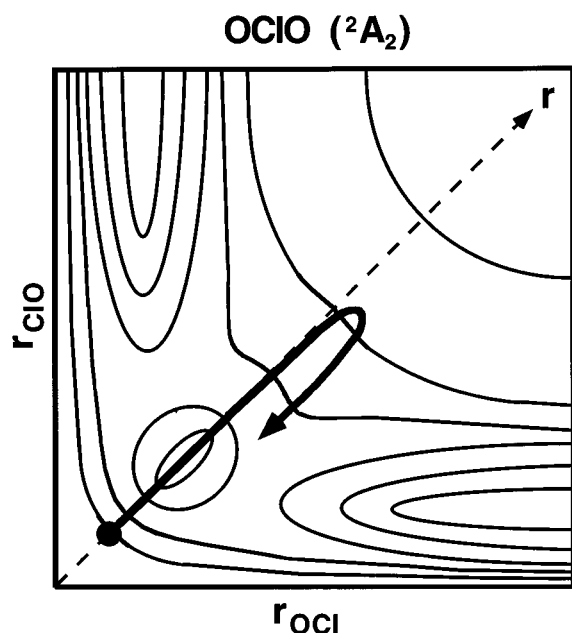


FIG. 11. A schematic of the two-dimensional $\tilde{A}(^2A_2)$ PES of OCIO. The dot marks the Franck-Condon region and the arrow indicates the initial motion of the localized wave packet along the symmetric stretching motion (see the text).

The independence of E_T and E_{int} of the fragments found in our experiments (see Fig. 10) is consistent with this expectation.

The rotational excitation of the ClO fragment has been found to be moderate¹³ and no indication from the present results points to an increase in E_{rot} with increased excitation energy; on the contrary, the $P(E_{\text{int}})$ distribution in Fig. 6 revealed a decrease at high fragment vibrational excitation. The PES(α, r) along the α bending coordinate in the inner region is therefore expected to show a small gradient giving rise to only a small torque $\partial V(\alpha, r)/\partial \alpha$. The narrow bands of the $(\nu_1, 0, 0)$ progression in the absorption spectrum reflect a long-lived resonance structure which in the time-dependent picture means a long residence time of the wave packet in the inner PES region. Thus the measured lifetimes correspond to more than ~ 10 vibrational periods of the excited state ν_1 mode. Once the barrier is crossed the fragments separate rapidly. Assuming a weak exit channel interaction the fragment internal energy distribution is essentially completed after having crossed the top of the barrier, i.e., the asymptotic or final rotational-vibrational state distribution reflects the transition state wave function of these coordinates.⁴⁵ Consequently the barrier energy with respect to the exit channel is deposited into translational motion of the fragments. In view of our experimental findings that E_T remains almost constant while E_{int} increases considerably with increasing excitation energy (Fig. 10), an exit channel interaction between these degrees of freedom is inefficient. Based on these considerations the barrier height can be estimated as illustrated in Fig. 12. From the average translational energy release, which was measured to be ≈ 52 kJ/mol at lower excitation energy, the dissociation energy of 247 kJ/

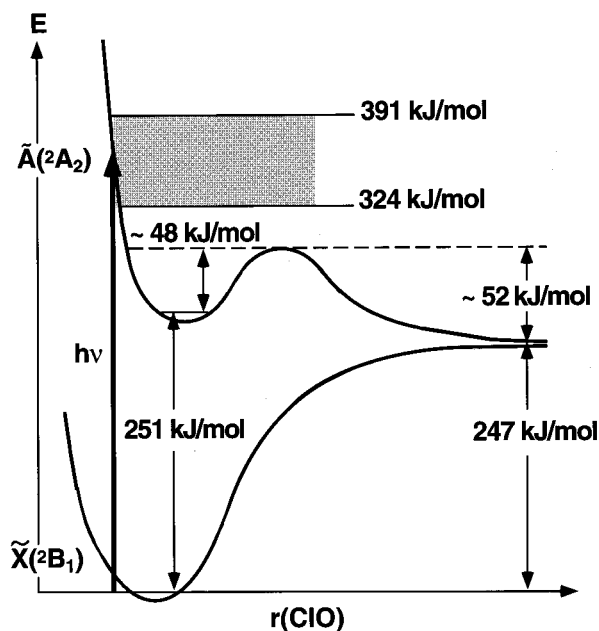
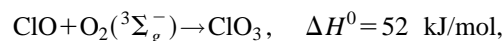


FIG. 12. Cut through the schematic $\tilde{X}(^2B_1)$ and $\tilde{A}(^2A_2)$ PESs of OCIO along the Cl-O bond coordinate. From the dissociation energy of reaction (1), $D_0=247$ kJ/mol, the energy of the $\tilde{A} \leftarrow \tilde{X}$ origin $E(0-0)=251$ kJ/mol (Ref. 17), and the measured translational energy $\langle E_T \rangle \sim 52$ kJ/mol, an inner barrier height of ~ 48 kJ/mol is estimated. The range of excitation energies (324–391 kJ/mol) is indicated by the shadowed region.

mol and the $\tilde{A} \leftarrow \tilde{X}(0-0)$ transition energy of 251 kJ/mol, a barrier height of ~ 4000 cm^{-1} (48 kJ/mol) is obtained.

C. Atmospheric chemistry

Due to its catalytic destruction of ozone in the stratosphere, the ClO radical is an important species in stratospheric chemistry.^{3,4,6,46,47} It appears generally accepted that the photolysis of the ClO dimer is the dominant chemical reaction responsible for the loss of O_3 in the antarctic. However, in regions of lower ClO concentrations this mechanism is less important simply because the $(\text{ClO})_2$ concentration depends on the square of the ClO concentration. In such atmospheric regions other O_3 loss pathways which involve, e.g., vibrationally highly excited ClO may gain importance. These hot radicals could provide the internal energy necessary to overcome bimolecular reaction barriers not accessible with cold radicals. According to our measurements, photolysis of OCIO at, e.g., the $(18,0,0)$ level in $\tilde{A} \ ^2A_2$ state provides 50% of nascent ClO fragments with an internal energy >96 kJ/mol and 10% >137 kJ/mol (see Table I). Vaida and Simon^{3,5,6} have suggested that the reaction of ClO with O_3 can be strongly enhanced at high internal energies of ClO. Other endothermic reactions pertinent to atmospheric chemistry such as⁴⁸



might also become important at high internal energies.

V. CONCLUSION

The photodissociation of OCIO according to reaction (1) is a predissociative process after excitation to the \tilde{A}^2A_2 state. The previous and present experimental results can be interpreted in a simplified manner in terms of a dissociation confined to the initial 2A_2 PES and thus neglecting interactions with the neighboring states 2B_2 and 2A_1 .^{14,23} Reduced to the two $r(\text{O}-\text{Cl})$ coordinates, the schematic PES (Fig. 11) is characterized by a well in the Franck-Condon region, which is separated by a small barrier estimated to be $\sim 4000 \text{ cm}^{-1}$ from the repulsive exit channel. The excitation energies E_{exc} used in the present study exceed this barrier and give rise to a ClO vibrational energy distribution which becomes extremely broad [$\nu(\text{ClO}) \sim 1-16$] with increasing E_{exc} . While the average translational energy of the fragment remains almost constant, the increase in photoenergy is channeled predominantly into E_{vib} of ClO. This behavior is reminiscent of the S_1 photodissociation of methylnitrite $\text{CH}_3\text{ONO} \rightarrow \text{CH}_3\text{O} + \text{NO}$ where a similar PES topology, although not symmetric with respect to two equivalent reaction coordinates, creates similar features of the fragment energy partitioning.³⁰ This is particularly striking when E_{trans} , E_{vib} , and E_{rot} for the CH_3ONO photodissociation given in Table 8 of Ref. 49 are compared to the corresponding data in Table I. The decoupling between the translational and vibrational degrees of freedom of the fragments is also pronounced in CH_3ONO .

The reduced β values relative to β_{max} can be attributed to a relatively long lifetime τ of the excited molecule prior to dissociation. The observed increase of β with increasing E_{exc} is thus due to a shortening of τ which is estimated to be from about 2.5 ps (9, 0, 0) to 0.45 ps (17, 0, 6). Within our simplified picture, the relatively long lifetime reflects the residence time of the wave packet within the well of the 2A_2 PES around the excitation (FC) region. Its oscillations, mainly along the symmetric stretching coordinate, give rise to the well-structured absorption spectrum.

Finally, the surprisingly strong vibrational excitation of the ClO fragment, which is manifested by a broad TOF spectra (Figs. 5 and 6), can contribute a considerable amount of internal energy to a bimolecular reaction. It is therefore conceivable that atmospheric reactions involving ClO may strongly be enhanced if the excitation conditions used in this studied prevail in the atmosphere.

ACKNOWLEDGMENTS

Support of this work by the Schweizerischer Nationalfonds zur Förderung der wissenschaftlichen Forschung is gratefully acknowledged. We thank Rolf Pfister for synthesizing OCIO, Dr. Gregory Hall for valuable discussions, and Dr. Robert T. Carter for critically reading the manuscript.

¹ S. Solomon, R. R. Garcia, F. S. Rowland, and D. J. Wuebbels, *Nature* **321**, 755 (1986).

² M. J. Molina and F. S. Rowland, *Nature* **249**, 810 (1974).

³ L. T. Molina and M. J. Molina, *J. Phys. Chem.* **91**, 433 (1987).

⁴ M. J. Molina, T.-L. Tso, L. T. Molina, and F. C.-Y. Wang, *Science* **238**, 1253 (1987).

⁵ J. D. Butler, *Air Pollution Chemistry* (Academic, London, 1979).

⁶ V. Vaida and J. D. Simon, *Science* **268**, 1443 (1995).

⁷ H. F. Davis and Y. T. Lee, *J. Phys. Chem.* **96**, 5681 (1992).

⁸ V. Vaida, S. Solomon, E. C. Richard, E. Rühl, and A. Jefferson, *Nature* **342**, 405 (1989).

⁹ V. Vaida, E. C. Richard, A. Jefferson, L. A. Cooper, R. Flesch, and E. Rühl, *Ber. Bunsenges. Phys. Chem.* **96**, 391 (1992).

¹⁰ E. Bishenden and D. J. Donaldson, *J. Chem. Phys.* **99**, 3129 (1993).

¹¹ E. Bishenden and D. J. Donaldson, *J. Chem. Phys.* **101**, 9565 (1994).

¹² T. Baumert, J. L. Herek, and A. H. Zewail, *J. Chem. Phys.* **99**, 4430 (1993).

¹³ R. F. Delmdahl, S. Baumgärtel, and K.-H. Gericke, *J. Chem. Phys.* **104**, 2883 (1996).

¹⁴ S. Michielsen, A. J. Merer, S. A. Rice, F. A. Freed, and Y. J. Hamada, *J. Chem. Phys.* **74**, 3089 (1981).

¹⁵ D. A. McDonald and K. K. Innes, *Chem. Phys. Lett.* **59**, 562 (1987).

¹⁶ E. C. Richard and V. Vaida, *J. Chem. Phys.* **94**, 163 (1991).

¹⁷ H. F. Davis and Y. T. Lee, *J. Chem. Phys.* **105**, 8142 (1996).

¹⁸ A. Arkell and I. Schwager, *J. Am. Chem. Soc.* **89**, 5999 (1967).

¹⁹ F. J. Adrian, J. Bohandy, and B. F. Kim, *J. Chem. Phys.* **85**, 2692 (1986).

²⁰ K. Johnsson, A. Engdahl, P. Ouis, and B. Nelander, *J. Mol. Chem.* **293**, 137 (1993).

²¹ H. S. P. Müller and H. Willner, *J. Phys. Chem.* **97**, 10589 (1993).

²² J. L. Gole, *J. Phys. Chem.* **84**, 1333 (1980).

²³ K. A. Peterson and H.-J. Werner, *J. Chem. Phys.* **96**, 8948 (1992).

²⁴ G. E. Busch, R. T. Mahoney, R. I. Morse, and K. R. Wilson, *J. Chem. Phys.* **51**, 449 (1969).

²⁵ A. M. Wodtke and Y. T. Lee, in *Molecular Photodissociation Dynamics*, edited by M. N. R. Ashfold, J. E. Baggott (Royal Society of Chemistry, London, 1987), pp. 31.

²⁶ M. N. R. Ashfold, I. R. Lambert, D. H. Mordaunt, G. P. Morley, and C. M. Western, *J. Phys. Chem.* **96**, 2938 (1992).

²⁷ P. Felder, *Chimia* **48**, 43 (1994).

²⁸ P. Felder, *Chem. Phys.* **143**, 141 (1990).

²⁹ P. Felder, Habilitation, University of Zürich, 1993.

³⁰ R. I. Derby and W. S. Hutchinson, *Inorg. Synth.* **4**, 152 (1953).

³¹ T. K. Minton, P. Felder, R. J. Brudzynski, and Y. T. Lee, *J. Chem. Phys.* **81**, 1759 (1984).

³² M.-A. Thelen, P. Felder, and J. R. Huber, *Chem. Phys. Lett.* **213**, 275 (1993).

³³ P. Felder, *Chem. Phys.* **155**, 435 (1991).

³⁴ J. G. Frey and P. Felder, *Mol. Phys.* **75**, 1419 (1992).

³⁵ S. Hubinger and J. B. Nee, *Chem. Phys.* **181**, 247 (1994).

³⁶ R. K. Sparks, K. Shobatake, L. R. Carlson, and Y. T. Lee, *Chem. Phys.* **75**, 3838 (1981).

³⁷ The dissociation energy of ClO^+ was calculated by subtracting the ionization energy (10.85 eV) of ClO from the sum of the dissociation energy (2.75 eV) of ClO and the ionization energy of Cl (13.0 eV), yielding a value of 4.9 eV (473 kJ/mol).

³⁸ K. P. Huber and G. Herzberg, *Molecular Spectra and Molecular Structure IV. Constants of Diatomic Molecules* (Van Nostrand Reinhold, New York, 1979).

³⁹ C. Jonah, *J. Chem. Phys.* **55**, 1915 (1971).

⁴⁰ R. N. Zare, *Mol. Photochem.* **4**, 1 (1972).

⁴¹ G. Busch and K. R. Wilson, *J. Chem. Phys.* **56**, 3626 (1972).

⁴² S. Yang and R. Bersohn, *J. Chem. Phys.* **61**, 4400 (1974).

⁴³ V. P. Hradil, T. Suzuki, S. A. Hewitt, P. L. Houston, and B. J. Whitaker, *J. Chem. Phys.* **99**, 4455 (1993).

⁴⁴ E. C. Richard, C. T. Wickham-Jones, and V. Vaida, *J. Phys. Chem.* **93**, 6347 (1989).

⁴⁵ R. Schinke, *Photodissociation Dynamics* (Cambridge University Press, Cambridge, 1993).

⁴⁶ M. Finkenbeiner, J. N. Crowley, O. Horie, R. Müller, G. K. Moortgat, and P. J. Crutzen, *J. Phys. Chem.* **99**, 16264 (1995).

⁴⁷ R. Atkinson, D. L. Baulch, R. A. Cox, R. F. Hampson, J. A. Kerr, and J. Troe, *J. Phys. Chem. Ref. Data* **18**, 881 (1989).

⁴⁸ U. Brühlmann, J. R. Huber, *Z. Phys. D* **7**, 1 (1987).

⁴⁹ A. Untch, R. Schinke, R. Cotting, and J. R. Huber, *J. Chem. Phys.* **99**, 9553 (1993).